Bone Reports 5 (2016) 243–251

Contents lists available at ScienceDirect

Bone Reports

journal homepage: www.elsevier.com/locate/bonr

Estrogen depletion and drug treatment alter the microstructure of type I collagen in bone

Meagan A. Cauble [a], Matthew J. Muckley [b], Ming Fang [a], Jeffrey A. Fessler [b,c], Kathleen Welch [d], Edward D. Rothman [d,e], Bradford G. Orr [f], Le T. Duong [g], Mark M. Banaszak Holl [a,b,h,*]

[a] Department of Chemistry, University of Michigan, Ann Arbor, MI, USA
[b] Department of Biomedical Engineering, University of Michigan, Ann Arbor, MI, USA
[c] Department of Electrical Engineering and Computer Science, University of Michigan, Ann Arbor, MI, USA
[d] Center for Statistical Consultation and Research (CSCAR), University of Michigan, Ann Arbor, MI, USA
[e] Department of Statistics, University of Michigan, Ann Arbor, MI, USA
[f] Department of Physics, University of Michigan, Ann Arbor, MI, USA
[g] Bone Biology Group, Merck Research Laboratories, West Point, PA, USA
[h] Macromolecular Science and Engineering, University of Michigan, Ann Arbor, MI, USA

ARTICLE INFO

Article history:
Received 28 July 2016
Received in revised form 15 August 2016
Accepted 25 August 2016
Available online 27 August 2016

Keywords:
Osteoporosis
OVX
Bisphosphonate
Cathepsin K inhibitor
AFM
Collagen

ABSTRACT

The impact of estrogen depletion and drug treatment on type I collagen fibril nanomorphology and collagen fibril packing (microstructure) was evaluated by atomic force microscopy (AFM) using an ovariectomized (OVX) rabbit model of estrogen deficiency induced bone loss. Nine month-old New Zealand white female rabbits were treated as follows: sham-operated (Sham; $n = 11$), OVX + vehicle (OVX + Veh; $n = 12$), OVX + alendronate (ALN, 600 μg/kg/wk., s.c.; $n = 12$), and OVX + cathepsin-K inhibitor L-235 (CatKI, 10 mg/kg, daily, p.o.; $n = 13$) in prevention mode for 27 weeks. Samples from the cortical femur and trabecular lumbar vertebrae were polished, demineralized, and imaged using AFM. Auto-correlation of image patches was used to generate a vector field for each image that mathematically approximated the collagen fibril alignment. This vector field was used to compute an information-theoretic entropy that was employed as a quantitative fibril alignment parameter (FAP) to allow image-to-image and sample-to-sample comparison. For all samples, no change was observed in the average FAP values; however significant differences in the distribution of FAP values were observed. In particular, OVX + Veh lumbar vertebrae samples contained a tail of lower FAP values representing regions of greater fibril alignment. OVX + ALN treatment resulted in a FAP distribution with a tail indicating greater alignment for cortical femur and less alignment for trabecular lumbar vertebrae. OVX + CatKI treatment gave a distribution of FAP values with a tail indicating less alignment for cortical femur and no change for trabecular lumbar vertebrae. Fibril alignment was also evaluated by considering when a fibril was part of discrete bundles or sheets (classified as *parallel*) or not (classified as *oblique*). For this analysis, the percentage of *parallel* fibrils in cortical femur for the OVX group was 17% lower than the Sham group. OVX + ALN treatment partially prevented the proportion of *parallel* fibrils from decreasing and OVX + CatKI treatment completely prevented a change. In trabecular lumbar vertebrae, there was no difference in the percentage of *parallel* fibrils between Sham and any of the other treatment groups.

1. Introduction

Chronic reduction of estrogen levels is known to negatively impact bone quality and increase the likelihood of fracture for over 75 million people worldwide, including 54 million people and 1.5 million fractures per year in the United States alone (Johnell and Kanis, 2006; Viguet-Carrin et al., 2006; Black and Rosen, 2016; Wright et al., 2014). The widespread prevalence of the osteoporosis and osteopenia diseases induced by estrogen reduction in postmenopausal women has spurred a search for quantitative measures that can serve to probe the changes in bone structure and predict fracture. Bone mineral density (BMD) measurements have proven useful as a primary assay but are only indirectly sensitive to changes in collagen matrix structure and have limited predictive ability for bone fracture (Burr, 2002). The role(s) that reduced estrogen levels play in osteoporotic reduction of bone quality remain an area of active scientific research. Evidence points to important changes in collagen structure in addition to changes in bone mineralization and porosity. Changes to the fibril nanomorphology and the

* Corresponding author at: Department of Chemistry, University of Michigan, 930 N. University Avenue, Ann Arbor 48109, MI, USA.
E-mail address: mbanasza@umich.edu (M.M.B. Holl).

http://dx.doi.org/10.1016/j.bonr.2016.08.003

microarchitecture of fibril organization have been observed in bone (Wallace et al., 2010a; Cauble et al., 2015) and skin (Fang et al., 2012a). Changes in collagen structure induced by estrogen depletion are partially prevented by treatment with anti-resorptive drugs such as the bisphosphonates and cathepsin K inhibitors (CatKI). In estrogen-depleted sheep and rabbits we have observed: A) an increase in the skewness of the distribution of Type I collagen D-spacings; (Wallace et al., 2010a) B) a decrease in the number of fibrils associated with ordered bundle and sheet structures and a concomitant increase in the number of fibrils in a disordered environment (Cauble et al., 2015). For these reasons, analytical tools and automated image analysis methods that can assess changes in the collagen matrix as a function of estrogen reduction and drug treatment are highly desired (Fang and Banaszak Holl, 2013; Wallace, 2012).

In our previous work, we characterized the effect of ovariectomy-induced estrogen depletion (OVX) and long-term treatment with alendronate (ALN), a cathepsin-K inhibitor L-006235 (CatKI, L-235), and 17β-estradiol (ERT) administered in prevention-mode on collagen fibril organization in rabbit cortical bone by classification of fibrils as existing in *parallel* regions (bundles and sheets) or *oblique* regions (Cauble et al., 2015). When analyzed by this method, OVX treatment for 27 weeks resulted in a decrease in the percentage of collagen fibrils in the *parallel* classification in cortical femur. This microstructural change was partially prevented by treatment with ALN and fully prevented by treatment with CatKI. We now extend the *parallel*/*oblique* analysis to rabbit trabecular bone and introduce a new, fully automated method to characterize an image-level fibril alignment parameter (FAP) for type I collagen fibrils in cortical femur and trabecular lumbar vertebrae. The addition of trabecular bone is important to this study because it is remodeled faster than cortical bone and changes in bone mass due to estrogen reduction are more pronounced. For this reason, many studies focus on the trabecular bone as a key metric for developing biological and structural understanding of osteoporosis (Pennypacker et al., 2011).

In this study, we first focus on a comparison between the collagen fibril structure in cortical and trabecular bone and then extend the comparison to include OVX + Veh, OVX + ALN, and OVX + CatKI treatments. Ovariectomy or OVX is a common model used to induce estrogen depletion (Wallace et al., 2010a; Fang et al., 2012a; Frost and Jee, 1992; Kalu, 1991; Smith et al., 2009). ALN is an orally available nitrogen-containing bisphosphonate that functions by binding to bone mineral and inducing apoptosis after being taken in by osteoclasts (Drake et al., 2008). This mechanism of action eliminates osteoclasts and thus alters cell signaling between osteoclasts and osteoblasts that is critical to maintaining bone mass homeostasis. Recently, treatment with odanacatib, a novel specific inhibitor of cathepsin K, a collagenase highly expressed by osteoclasts, did not lead to reduction of osteoclast number in preclinical species and humans (Pennypacker et al., 2011). This drug is effective because cathepsin K is the primary collagenase in bone and plays an important role in osteoclast mediated bone resorption (Troen, 2004). The animal model used in this study consists of 9-month-old female New Zealand white rabbits chosen because of their similarities to humans with respect to the cathepsin K enzyme and Haversian remodeling in cortical bone (Cauble et al., 2015; Pennypacker et al., 2011). The treatment groups included Sham-operated + vehicle ($n = 11$), OVX + Veh ($n = 12$), OVX + ALN (600 μg/kg/wk., s.c.; $n = 12$) and OVX + CatKI (L-006236, 10 mg/kg, daily, p.o.; $n = 13$) in prevention mode for 27 weeks. Note, L-235 is structurally related and displays similar potency and selectivity as odanacatib in preclinical models of osteoporosis (Pennypacker et al., 2011).

We have imaged both cortical femur and trabecular lumbar vertebrae rabbit bone using atomic force microscopy (AFM). The image sets were analyzed using two approaches. First, individual fibrils with a measurable D-spacing in the images were coded as being present in local *parallel* or *oblique* arrangements using the method described previously (Cauble et al., 2015). For the first time, we have extended the imaging and the *parallel*/*oblique* analysis to trabecular bone with either OVX + Veh or OVX + drug treatment. This analysis approach relies on hand coding of the images, is very time consuming, omits fibrils without a measurable D-spacing, and is limited to the approximation of assigning fibrils with just two classifications. An automated image analysis that could function at the level of the entire image and provide a continuous variable characterizing the extent of fibril organization was highly desired. To achieve this goal, we developed a second analysis approach that employs autocorrelation of image patches to compute a vector field that approximates fibril alignment. We then used that vector field to generate a fibril alignment parameter (FAP) based on an information-theoretic entropy calculation for each image as well as to form maps indicating the spatial alignment within a given image. We applied this approach to both the cortical and trabecular sample sets.

Comparing the cortical to trabecular collagen structure, the percentage of fibrils in the *parallel* microstructure decreased and the percentage of *oblique* microstructures increased. The cortical and trabecular bone resulted in the same average FAP value; however, the distribution of FAP values derived from the individual regions contained more high FAP values (low alignment) for the trabecular case and low FAP values (high alignment) for the cortical case. Both observations are consistent with our qualitative assessment of the relative amount of fibril alignment observed for the two bone types. Treatment with OVX + ALN resulted in a shift towards lower FAP values for cortical bone and a partial prevention of the increase in the frequency of *oblique* fibrils; however, for trabecular bone higher FAP values were obtained coupled to an increase in the frequency of *parallel* coded microstructure. Treatment with OVX + CatKI resulted in a shift towards higher FAP values for cortical bone, with no change in the *parallel*/*oblique* classifications, and no change in FAP values for trabecular bone although the frequency of *parallel* coded microstructure increased similar to the OVX + ALN treatment. In summary, both image analysis approaches indicate that 1) cortical collagen and trabecular collagen alignment differs significantly and 2) OVX + Veh or treatment with either OVX + ALN or OVX + CatKI can impact the alignment of the collagen fibrils in both cortical and trabecular bone and 3) the impact of OVX + Veh, OVX + ALN, and OVX + CatKI treatment on collagen fibril alignment differs between the cortical and trabecular bone.

2. Materials and methods

2.1. Bone preparation and AFM imaging

All samples were obtained from Merck Research laboratories and stored in 95% ethanol (Cauble et al., 2015; Pennypacker et al., 2011). Rabbit cortical femur images analyzed were from our previously published data set (Cauble et al., 2015). There were a total of 663 images (3.5 μm^2) for cortical femur samples taken from 48 animals (11 Sham, 12 OVX + Veh, 12 OVX + ALN, and 13 OVX + CatKI). Image sampling methods were previously described in detail (Cauble et al., 2015). In all cases, cortical femur images are oriented such that the long bone axis is horizontal on the page. Trabecular bone from the lumbar vertebrae of the same animals was added to the current study. All images were obtained blind to treatment type. AFM imaging of the lumbar trabecular samples was quite challenging due to the heterogeneous organization of trabecular spicules and the fragility of the trabeculae. In this case, images were oriented such that the long trabecular axis is horizontal on the page. This does not correspond to an overall alignment with respect to the lumbar vertebra orientation. Methods development required an extended period and resulted in the loss of 1 Sham, 1 OVX + Veh, and 1 OVX + CatKI sample from the data set. The final animal counts for the lumbar vertebrae are as follows: Sham + vehicle ($n = 10$), OVX + Veh ($n = 11$), OVX + ALN ($n = 12$), and OVX + CatKI ($n = 12$). The lumbar vertebrae samples were prepared by sectioning a region of the caudal end and mounting onto a steel

AFM puck. Bone marrow was mechanically removed using forceps followed by polishing the sample on a wheel for 2–4 min using a 3-micron diamond suspension and sonication in nanopure water for 5 min to remove the polishing solution. The surface collagen was demineralized by shaking in 0.5 M EDTA pH = 8.0 for 30 min at room temperature. Sonication was repeated for 5 min prior to air drying before imaging in tapping mode. All imaging was performed in air at room temperature with a conical AFM probe (nanoScience Instruments; Aspire conical tapping mode AFM probes; 300 kHz, 40 N/m, radius 8 nm). Initial scans for trabecular lumbar vertebrae images were acquired using a 10 μm × 10 μm image area on a trabecular rod structure. A set of 3.5 μm × 3.5 μm images were acquired for each region with a total of 526 images (3.5 μm × 3.5 μm) available for the calculation of the fibril alignment parameters from the 45 animals. 3605 and 2187 fibrils and were identified for D-spacing measurement and coding as being in a *parallel* microstructure (bundle or sheet) or *oblique* microstructure for the cortical femur and trabecular lumbar vertebrae, respectively.

2.2. Analysis of D-spacing

The D-periodic axial/gap overlap spacing (D-spacing) was employed as a quantitative metric for changes in collagen fibril nanomorphology for the blinded lumbar trabecular bone samples. A total of 511 fibrils were measured for Sham, 662 for OVX + Veh, 533 for OVX + ALN, and 654 for OVX + CatKI. Full details on the instrument calibration, controls for instrument thermal drift, and the use of 2D-Fourier transforms to accurately measure the fibril D-spacing have been previously published (Wallace et al., 2010a; Wallace et al., 2010b; Erickson et al., 2013). We note that thermal instrument drift, instrument calibration and tilt angles in the D-spacing must be properly accounted for to obtain accurate distributions (Erickson et al., 2013; Fang et al., 2013) and that some tissues can exhibit a narrow range of D-spacing values over large regions as we (Fang et al., 2012b) and others have reported (Su et al., 2014).

2.3. Parallel and oblique fibril classification

Each fibril was coded as either *parallel* or *oblique* to assess the local microstructure surrounding individual collagen fibrils. This hand-coding was performed while blinded to treatment group. The *parallel*/*oblique* classification has been presented in detail previously. (Cauble et al., 2015) Briefly, fibrils were given the *parallel* classification if they existed in a bundle of 3–15 fibrils aligned in parallel to one another with defined edges or in a sheet of >20 parallel, aligned fibrils that are continuous with adjacent bone. An *oblique* classification was given when fibrils were in a microstructure with a wide range of fibril-fibril angular dispersion. Topography and amplitude images were both used for making this classification. The results of this analysis for the cortical femur have been previously reported (Cauble et al., 2015). This fibril-by-fibril analysis was implemented for the trabecular lumbar vertebrae in the same way it was for the cortical femur.

2.4. Fibril alignment parameter (FAP) calculation and analysis

To quantitatively assess the degree of fibril alignment in the AFM images, we developed and employed an autocorrelation approach and an information-theoretic entropy metric to determine a fibril alignment parameter (FAP). The FAP provides reproducible and quantitative image-to-image and sample-to-sample comparisons of the collagen fibril alignment. This autocorrelation approach was developed after the sample blinding had been removed. The images employed contain the data used for D-spacing and *parallel*/*oblique* fibril classifications. This analysis used amplitude images since this image mode highlights D-spacing and fibril-to-fibril features as opposed to overall topographic slope. A high pass FFT-based filter with a square-shaped frequency response of width 8000 nm^{-1} (i.e., excluding frequencies below 0.004 nm^{-1}) was applied to the images to prevent artifacts in the autocorrelation resulting from local variation in the amplitude gray scale within an image. A patch size of 64 × 64 pixels (439 × 439 nm) was selected, corresponding to a region containing six to seven D-spacings along a fibril length and about six to seven fibrils in width. An array of patches across each 3500 nm × 3500 nm image was created by shifts of 4 pixels in the x and y directions. Each patch in the array was then correlated with neighboring patches. The analysis performed a restricted search to obtain the maximum autocorrelation from patches in a shift range between 7 and 14 pixel shifts (corresponding to 48 nm to 96 nm; this is within the ~60–70 nm range of the repeated structures present from D-spacing and individual fibril widths). Each patch's orientation was represented by the vector that indicated the angle and magnitude of the highest neighboring patch correlation. A quiver plot overlaid on an AFM image illustrates the results of this process (See Supplemental material, Figs. S1 and S2).

We used a normalized information theoretic entropy value as a summary statistic for the (dis)similarity of all of the patch alignment vectors computed from a given image. The information-theoretic entropy is defined for a probability distribution function $p(x_j)$ as follows (Eq. (1)):

$$\varepsilon = -\sum_{j=1}^{J} p(x_j)\,\ln\left(p(x_j)\right), \tag{1}$$

where x_j is the center of a histogram bin of alignment angles and $p(x_j)$ is the probability of an alignment angle being in the bin corresponding to j. We let j range from 1 to J, where J = 40 is the number of histogram bins in this study. To define $p(x_j)$, we created a synthetic probability distribution based on the angles and lengths of the alignment vectors. The normalized entropy of this synthetic distribution yields a parameter that captures the extent of collagen fibril misalignments, due to the properties of the entropy function. For these entropy calculations, instead of using the usual empirical probability distribution of the alignment angles, we weighted the probability of an angle by the confidence in that alignment angle (Eq. (2)),

$$p(x_j) \triangleq \frac{\sum_{n\in s_j} \kappa_n}{\sum_{n=1}^{N} \kappa_n}, \tag{2}$$

where κ_n is the correlation between the patch at location n and its patch of maximum correlation, s_j is a set that collects all locations with angles in a bin around x_j, and N denotes the total number of patches. This calculation of the $p(x_j)$ values ensures that they take values between 0 and 1 and that they sum to 1 as required for a probability distribution function.

We define the FAP to be the entropy value in Eq. (1) normalized by (divided by) the entropy of a uniform distribution (which is the distribution having the highest possible entropy). The FAP value quantifies the degree of fibril *mis*alignment in the distribution of alignment angles. This is the FAP that is on a scale of 0 to 1 with 0 resulting from vectors that are completely aligned or parallel (same angle) and 1 resulting from fibrils that exhibit no dominant alignment. Furthermore, the FAP is insensitive to the number of bins used in the calculation of the probabilities due to the normalization by a uniform distribution.

3. Results

To gain a greater understanding of the differences between the collagen structure in cortical and trabecular bone, and between normal tissue and tissue affected by estrogen deficiency and by treatment with ALN or CatKI, we have compared cortical femur and trabecular lumbar vertebrae from Sham, OVX + Veh, OVX + ALN, and OVX + CatKI groups. Imaging the trabecular bone in the rabbit lumbar vertebrae was substantially more challenging than the imaging of the cortical femur bone. For the cortical femur region, the bone itself is robust and after polishing and demineralizing a large, continuous field of collagen

is available for study. As illustrated in Fig. 1, the center region of a lumbar vertebrae contains trabecular spicules separated by large gaps that had been filled with marrow. Imaging regions were selected on the trabeculae, which even after polishing remained rough on the micron scale as compared to similarly prepared cortical femur bone. Exemplar pictures of both the cortical femur and lumbar vertebrae are provided in Fig. S3. The presentation of results is organized in terms of increasing hierarchical structural scale. We first focus on changes in the D-spacing values within fibrils. The presentation then turns to a hand coded analysis of the local fibril organization for each of the fibrils assessed for its D-spacing value. Finally, we present a newly developed analysis where we quantify the fibril alignments in a 3.5 × 3.5 μm image field. Thus, our structural analysis starts on a ~50–100 nm scale, progresses to a ~70–700 nm scale, and ends assessing alignment over a 3500 nm region.

3.1. Analysis of D-spacing variation

No changes were observed in the overall D-spacing distributions for either the rabbit cortical or trabecular samples as a function of estrogen deficiency or drug treatment (Fig. S4, see Cauble et al. (2015) for cortical femur data). The average values were 65.9, 65.4, 64.9, and 64.8 nm (0.5 nm standard error) for Sham, OVX + Veh, OVX + ALN, and OVX + CatKI, respectively with D-spacings ranging from about 57–75 nm for the trabecular lumbar vertebrae samples. By way of comparison, the average values were 62.6, 63.9, 63.6, and 62.7 nm for Sham, OVX + Veh, OVX + ALN, and OVX + CatKI, respectively with D-spacings ranging from about 57–70 nm for the cortical femur samples (Cauble et al., 2015). Although no difference in D-spacing was observed when considering all data, an interesting animal-to-animal effect was present when considering fibrils coded as bundles.

3.2. Analysis of animal-to-animal variability in bundle D-spacing

We examined the distribution in D-spacing that exists for fibrils coded as existing in bundles only and in this way excluded the very disperse 50% or so of measurements arising from the more heterogeneous *oblique* fibrils as well as fibrils coded as existing in a sheet microstructure. In trabecular lumbar vertebrae, there were no significant differences among the means across treatments ($p = 0.46$) (Fig. 2). However, there were significant differences in the degree of animal-to-animal variability across treatment groups ($p = 0.02$ by likelihood ratio test). Fitting a variance components model within each treatment, including a random effect for animal, there is zero variability estimated between rabbits in the Sham group. The OVX + Veh group exhibited a non-significant animal-to-animal variability in the D-spacing of trabecular fibrils coded as being in a bundle microstructure ($p = 0.074$; likelihood ratio chi-square test). Significant between animal variability was observed in both the OVX + ALN and OVX + CatKI treatment groups ($p < 0.01$ in each treatment). This analysis of bundle D-spacing was also performed for the cortical femurs (Fig. 3). A likelihood ratio test for the equality of the variances showed that there were no significant differences in animal-to-animal variability across the four treatments for the cortical femurs ($p = 0.64$). Treatment with ALN or CatKI introduced animal-to-animal variability in the bundle D-spacing values for trabecular bone and not cortical bone.

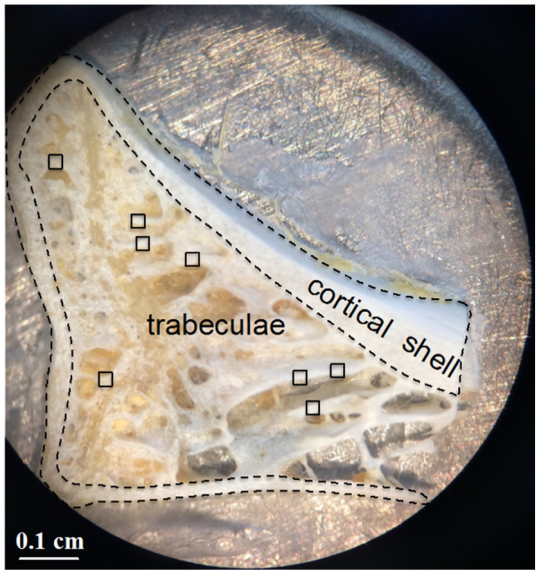

Fig. 1. Optical image of rabbit lumbar vertebrae section. AFM images were obtained at the polished top edge of the trabeculae. Examples of such areas are indicated by the square regions of interest (□).

3.3. Parallel and oblique fibril classification

We compared the percentage of fibrils coded as *parallel* in trabecular versus cortical bone within each treatment group using a Generalized Estimating Equation (GEE) approach (Diggle et al., 2002) that takes into account the correlation among observations in the same animal (Table 1). All fibrils quantified in terms of D-spacing values were hand-coded as existing in either *parallel* or *oblique* microstructures. The cortical bone OVX + Veh group had a percentage of *parallel* fibrils that was 12% lower than the trabecular bone from the same group and this difference was marginally significant ($p = 0.06$). All other comparisons for the percentage of *parallel* fibrils were non-significant ($p > 0.05$). The same comparisons for the percentage of *oblique* fibrils were also non-significant ($p > 0.05$). All comparisons with their p-values can be found in Tables S1 and S2.

We also compared the percentage of fibrils coded as *parallel* in cortical and trabecular bone between treatment groups. As previously described, (Cauble et al., 2015) the percentage of *oblique* fibrils in rabbit cortical femur was estimated to be 18% greater in the OVX + Veh group than in the Sham group ($p = 0.003$). However, the percentage of *oblique* fibrils in rabbit trabecular lumbar vertebrae was 4% lower in the OVX + Veh than in the Sham group and this difference was non-significant ($p = 0.64$). All differences in the percentage of fibrils in a given microstructure for trabecular bone were non-significant ($p > 0.05$). The OVX + CatKI has 13% more fibrils coded as *parallel* than the Sham group and this was the largest difference observed in the trabecular bone ($p = 0.11$).

3.4. Fibril alignment parameter analysis of AFM images from cortical femur and trabecular lumbar vertebrae

Our previous observations that estrogen deficiency and drug treatment impact collagen structure in bone, (Cauble et al., 2015) and that the dispersion of D-spacing values was affected by the collagen packing microstructure, (Fang et al., 2012b) drove our interest in developing quantitative approaches to the analysis of the fibril packing on a multi-micron scale. The new approach presented here has the advantages of being fully automated, avoiding the tedious nature of the blinded hand coding, and generates average alignment parameter values that vary continuously from 0 (fibrils aligned in parallel) to 1 (fibrils exhibit no dominant alignment) for each image. This quantitative output allows ready comparison of images both within and between sample sets.

Fibril alignment parameter (FAP) calculations were performed for a total of 663 images for cortical femur samples and 526 images for trabecular lumbar vertebrae samples across 48 animals (3.5 μm × 3.5 μm). The average FAP values for sham femur and sham lumbar vertebrae were the same (0.9 ± 0.1); however, the distributions of the FAPs differed with the cortical femur having more images in the 0.4 to 0.8 parameter range (more alignment) and fewer images in the 0.9 to 1.0 range (less alignment) (Fig. 4). The histograms are not Gaussian distributions and

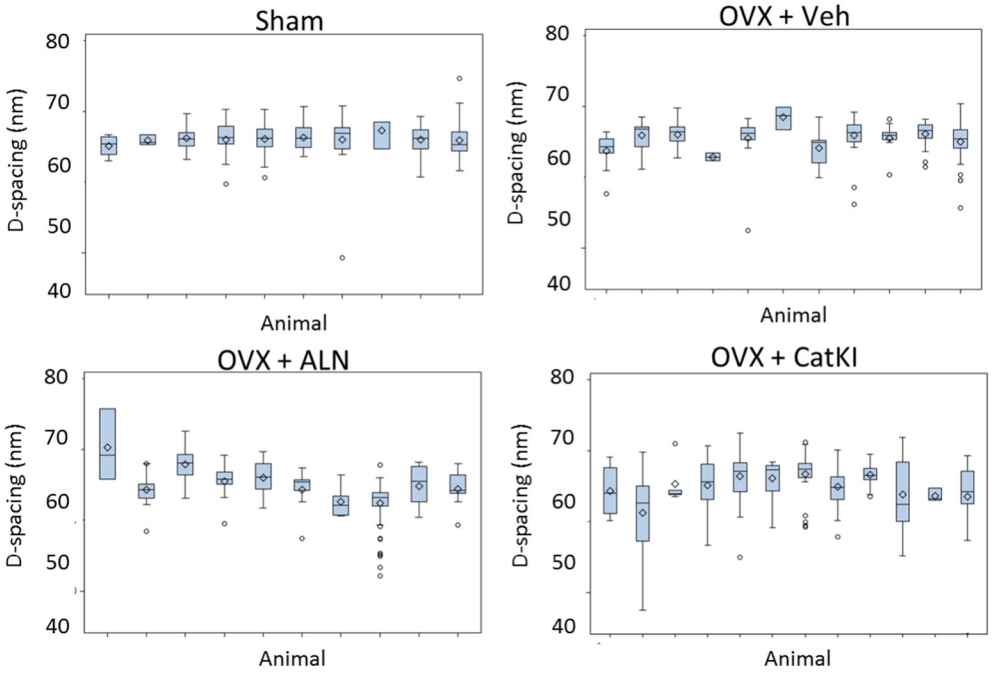

Fig. 2. Boxplots of the D-spacing distribution of the collagen fibrils located in trabecular bundles obtained for Sham, OVX + Veh, OVX + ALN, and OVX + CatKI groups. There are significant differences in the degree of animal-to-animal variability across treatments in trabecular bone ($p = 0.02$, likelihood ratio Chi square test). The animal-to-animal variance for the OVX + Veh treatment was marginally significant ($p = 0.074$). Both of the drug treatments introduced significant animal-to-animal variability in the bundle D-spacing ($p < 0.01$). There were two ALN animals that did not contain any fibrils that were coded as being in a bundle. One of those two animals had both sheet and *oblique* microstructures and the other animal only had *oblique* microstructures.

were plotted as cumulative distribution functions to perform statistical comparisons. Exemplar images are provided in Fig. 4b along with the CDF to illustrate how changes in image-level fibril alignment correspond to the changes in FAP. A Kolmogorov-Smirnov (K-S) test, which is sensitive to changes in distribution mean and width and does not require normally distributed data, (Erickson et al., 2013) indicated the cortical and trabecular distributions for Sham tissue were significantly different ($p < 0.01$).

3.5. Effect of estrogen deficiency on FAP distributions in cortical femur and trabecular lumbar vertebrae

Sham and OVX + Veh animals showed no difference in their average FAP (0.8 ± 0.1) or distribution of values ($p = 0.48$ for cortical femur; $p = 0.07$ for trabecular vertebrae) (Fig. 5a and b). Although Sham cortical and Sham trabecular bone exhibit significantly different FAP distributions ($p < 0.01$), in response to OVX + Veh the lumbar vertebrae

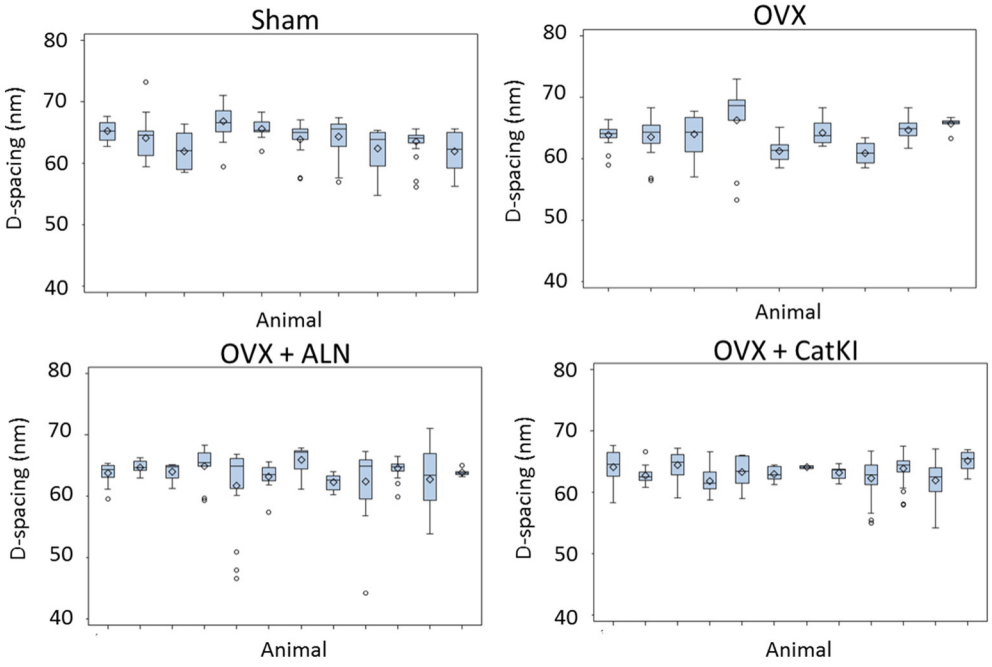

Fig. 3. Boxplots of the D-spacing distribution of collagen fibrils located in cortical femur bundles obtained for Sham, OVX + Veh, OVX + ALN, and OVX + CatKI groups. There were no significant differences in the animal-to-animal variability across the four treatment groups ($p = 0.64$, likelihood ratio test).

Table 1
Percentage of type I collagen fibrils observed in *parallel* and *oblique* microstructures.

Treatment		# of fibrils	# of animals	Percentage in *parallel* microstructures (%, std error)	Percentage in *oblique* microstructures (%, std error)
Cortical Femur	Sham	825	11	52 (5)	45 (5)
	OVX + Veh	808	12	35 (5)	63 (5)
	ALN	971	12	40 (5)	57 (5)
	CatKI	1001	13	47 (5)	49 (5)
Trabecular Lumbar Vertebrae	Sham	511	10	44 (7)	56 (7)
	OVX + Veh	662	11	47 (5)	52 (5)
	ALN	532	12	46 (6)	53 (6)
	CatKI	654	12	57 (5)	43 (5)

FAP distribution moves towards that of the cortical femur distribution and the two CDFs are no longer statistically different ($p = 0.15$) (Fig. 6a). Recall that the comparison between Sham and OVX + Veh rabbits for cortical femur did show a statistically significant difference in microstructure when considering the classification into *parallel* and *oblique* structures (Table 1) (Cauble et al., 2015). The FAP values for the lumbar trabecular bone were 0.9 ± 0.1 for Sham and 0.8 ± 0.1 for OVX + Veh. The distribution of values from OVX + Veh shifted slightly to higher alignment; however, the shift is marginally significant as assessed by the K-S statistic ($p = 0.07$) (Fig. 5b).

3.6. Effects of ALN and CatKI drug treatments on FAP distributions in cortical femur and trabecular lumbar vertebrae

Drug treatments did not change the average FAP values of 0.8 ± 0.1 and 0.9 ± 0.1, respectively, for the cortical femur and trabecular lumbar vertebrae, but they did affect the distributions (Fig. 5). For the cortical femur groups, OVX + ALN treatment resulted in a significant increase in the number of regions of parallel alignment (decrease in FAP) as compared to OVX + Veh ($p = 0.01$). Treatment with OVX + CatKI resulted in a significant decrease in the number of regions of parallel alignment (increase in FAP) as compared to Sham ($p < 0.01$) and OVX + ALN ($p < 0.01$) but not to OVX + Veh ($p = 0.08$). For the trabecular lumbar vertebrae data, the OVX + ALN treatment resulted in a significant decrease in the numbers of regions of parallel alignment (increase in FAP) as compared to OVX + Veh ($p < 0.01$). Treatment with OVX + CatKI also resulted in a significant decrease in the numbers of regions of parallel alignment (increase in FAP) as compared to OVX ($p = 0.01$). The change in FAP distribution as a function of bone type and drug treatment is summarized in Fig. 5c. For any given treatment, the change in FAP distribution relative to Sham is different for cortical and trabecular bone.

4. Discussion

In this study, we have expanded our previous work on changes in collagen structure induced by OVX, OVX + ALN, and OVX + CatKI treatments on the cortical femur bone of rabbit (Cauble et al., 2015) to the trabecular lumbar vertebrae and we introduce a new, image level, quantitative analysis of the impact on fibril alignment in both types of bone. Trabecular bone in the vertebrae is a complex tissue composed of a bicontinuous network of mineralized collagen trabeculae interspersed with marrow (Fantner et al., 2006). Previous AFM studies on trabecular bone have noted the complexity of the woven collagen fibrils do not seem to match a simple twisted plywood model of fibril orientation and alignment (Hassenkam et al., 2004). AFM images of human osteoporotic trabecular bone from a fractured femoral head have been reported; however, the medication history of the individual is not known (Hassenkam et al., 2005).

4.1. D-spacing variation

In five-year-old Columbia-Rambouillet cross sheep, ovariectomy-induced estrogen depletion induces changes in type I collagen D-spacing distributions (Wallace et al., 2010a). Wallace et al. concluded that OVX (3 animals; 182 fibrils) resulted in a decrease in the mean D-spacing and a shift in the overall D-spacing distribution towards lower values in ovine bone ($p < 0.001$) when compared to the Sham treatment group (3 animals; 168 fibrils). For these rabbit cortical and trabecular samples, no changes were observed in the overall D-spacing distributions (Fig. S4, see Cauble et al. (2015) for cortical femur data). The rabbits used were skeletally mature (rabbits reach skeletal maturity by eight months) (Castaneda et al., 2008). In addition, the rabbits were sacrificed 27 weeks after ovariectomy (about 3 remodeling cycles), which is sufficient time to observe reduction in bone mass induced by estrogen depletion (Pennypacker et al., 2011). In the ovine study, the

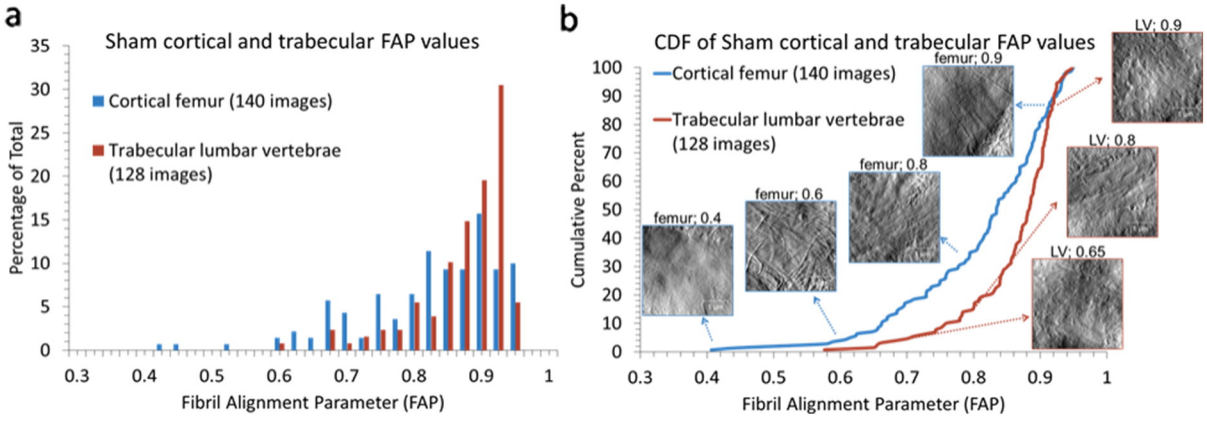

Fig. 4. Distribution of FAP values in cortical and trabecular bone in sham-operated rabbits. a) Cortical femur and trabecular lumbar vertebrae in Sham exhibit a non-Gaussian distribution of FAP values with an average value of 0.8 ± 0.1. b) Cumulative distribution functions of FAP values for cortical femurs and trabecular lumbar vertebrae in Sham. The Sham lumbar vertebrae were shifted towards higher FAP values (less collagen alignment) with statistical significance ($p < 0.01$).

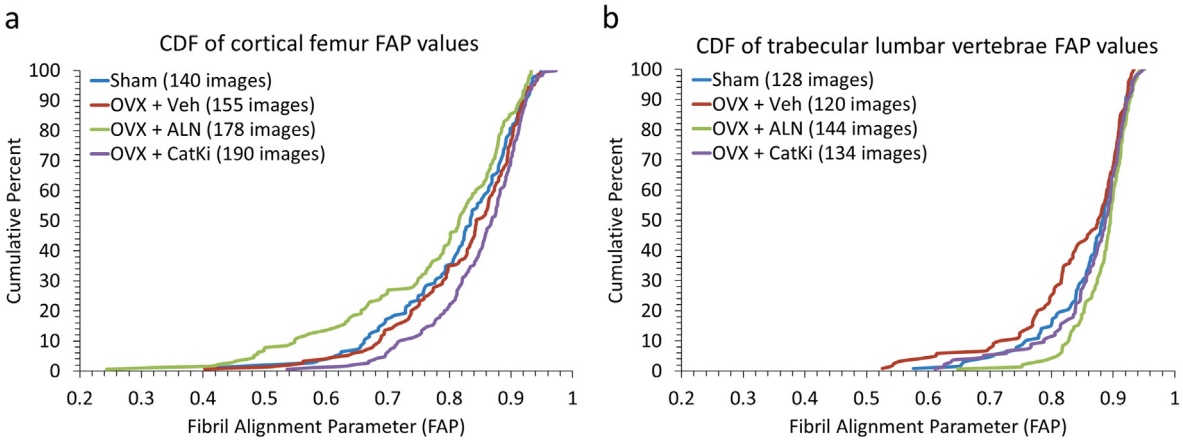

c

	Cortical femur	Trabecular lumbar vertebrae
OVX + Veh	no change in FAP	shift FAP to lower values
OVX + ALN	shift FAP to lower values	shift FAP to higher values
OVX + CatKI	shift FAP to higher values	no change in FAP

Fig. 5. Distribution of FAP values for Sham, OVX + Veh, and OVX + drug treated bone in cortical femur (a) and trabecular lumbar vertebrae (b). All eight groups had the same average FAP value (0.8 ± 0.1 for cortical Sham, cortical OVX + Veh, cortical OVX + ALN, and trabecular OVX + Veh and 0.9 ± 0.1 for cortical OVX + CatKI, trabecular Sham, trabecular OVX + ALN, and trabecular OVX + CatKI). (a) For cortical bone, the distribution of FAP values showed no statistically significant change after ovariectomy ($p = 0.48$). In comparison to Sham, drug treatment after ovariectomy resulted in a shift towards more alignment ($p = 0.20$) with ALN treatment and less alignment (0.01) with CatKI treatment. (b) In comparison to Sham, the distribution of FAP values for OVX + Veh is shifted towards more alignment ($p = 0.07$), treatment with alendronate shifts towards less alignment ($p = 0.054$), and treatment with CatKI has little effect ($p = 0.89$). (c) A summary of these changes in comparison to Sham.

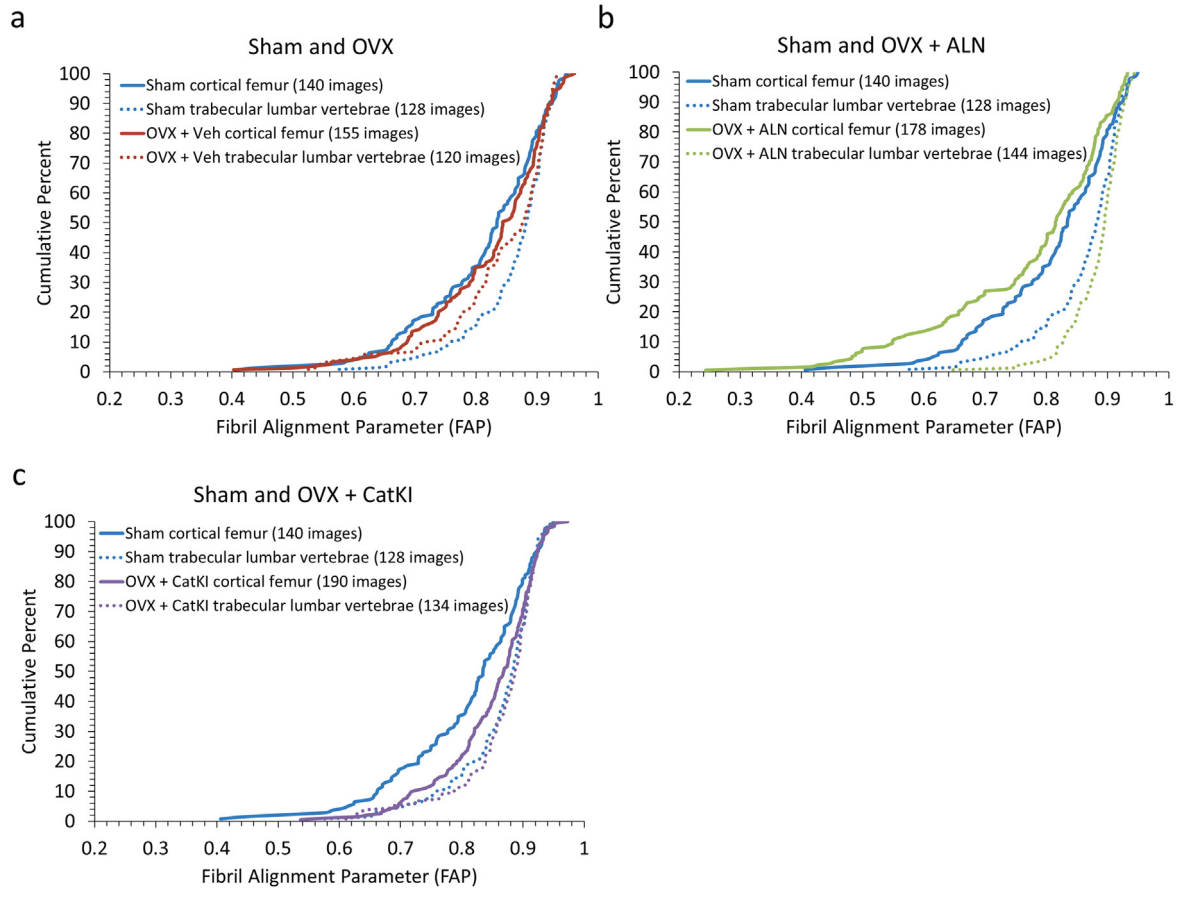

Fig. 6. Cumulative distribution function of FAP values for estrogen depleted and drug treated animals in data sets I and III. Ovariectomy resulted in no statistically significant change to the FAP distribution for cortical bone ($p = 0.48$) and a shift towards lower FAP (more alignment) in the trabecular bone ($p = 0.07$). Treatment with alendronate resulted in the trabecular bone becoming less aligned ($p = 0.054$) and the cortical bone becoming more aligned ($p = 0.20$). In contrast, treatment with CatKI showed no statistically significant change in extent of alignment for trabecular bone ($p = 0.89$) but did shift the cortical bone towards higher FAP value or less alignment ($p < 0.01$). When comparing the distributions between femur and lumbar vertebrae within a treatment group, OVX + Veh is the only group that does not have a significant difference (Sham, $p < 0.01$; OVX + Veh, $p = 0.15$; OVX + ALN, $p < 0.01$; OVX + CatKI, $p = 0.02$).

animals used by Wallace et al. were also skeletally mature and allowed to reach peak bone remodeling rates post-OVX. Markers for bone remodeling in sheep peak after 3–4 months (~1 remodeling cycle), but require about 12 months to observe bone mineral density loss (Komori, 2015). It is not clear if the different response to estrogen depletion is due to species dependent differences in bone loading and remodeling rates in rabbit versus sheep; or if the changes observed by Wallace et al. in ovine bone would be minimized with a larger sample size.

Although the rabbits did not exhibit a change in skewness of the D-spacing distribution when considering the overall distribution, the amount of animal-to-animal variation in the D-spacing of fibrils in the trabecular lumbar vertebrae coded as bundles was not the same for all four treatment groups (Fig. 2). The OVX + ALN and OVX + CatKI treatment groups had more animal-to-animal variability. There were no differences in the animal-to-animal variability of bundle D-spacing for the cortical femurs ($p = 0.64$). The faster remodeling rate of trabecular bone is one possible source of this observed difference between the two types of rabbit bone.

4.2. Parallel and oblique fibril classification

The only significant difference observed for the *parallel* and *oblique* collagen fibril classification is the large change in parallel microstructure observed for Sham vs. OVX + Veh rabbits for cortical femur ($p = 0.004$), an observation that was replicated with a fully independent rabbit experiment (Cauble et al., 2015). In comparing the results for cortical femur and trabecular lumbar vertebrae for the OVX + Veh group, the cortical bone had 12% fewer *parallel* fibrils than the trabecular bone ($p = 0.06$). This observation, although marginally significant, is still surprising at first glance since trabecular bone is expected to have less collagen alignment than trabecular bone. Indeed, this is the trend highlighted in Fig. 4. However, comparing the percentage of *parallel* microstructure in Sham rabbit cortical femur (52%) to Sham or OVX + Veh trabecular lumber vertebrae (44% and 47%, respectively) makes it clear that as expected, and consistent with Fig. 4, rabbit cortical femur has a greater degree of parallel coded collagen. What differs is the dramatic impact of estrogen deficiency on the parallel coded structure in cortical femur whereas no significant change is observed for the rabbit trabecular lumbar vertebrae. The largest difference observed for trabecular lumbar vertebrae was the 13% increase in *parallel* coded fibrils for the OVX + CatKI treatment group over the Sham group; however, this difference was not significant ($p = 0.11$).

4.3. Fibril alignment parameter (FAP)

Our previous observations that estrogen deficiency and drug treatment impact collagen structure in bone, (Cauble et al., 2015) and that the dispersion of D-spacing values was affected by the collagen packing microstructure, (Fang et al., 2012b) drove our interest in developing quantitative approaches to the analysis of the fibril packing on a multimicron scale. The new approach presented here has the advantages of being fully automated, avoiding the tedious nature of the blinded hand coding, and generates average alignment parameter values that vary continuously from 0 (fibrils aligned in parallel) to 1 (fibrils exhibit no dominant alignment) for each image. This quantitative output allows ready comparison of images both within and between sample sets.

Sham animals have significantly different FAP distributions for cortical and trabecular bone with cortical femur having lower FAP values (more aligned) and trabecular lumbar vertebrae having higher FAP values (less aligned). Estrogen deficiency in the OVX + Veh group shifts the trabecular distribution towards lower FAP values and the cortical and trabecular distributions are no longer significantly different from one another (Fig. 6). Treatment with ALN following ovariectomy impacts both cortical and trabecular bone with cortical bone shifting towards lower FAP values and trabecular bone shifting towards higher FAP values. Treatment with CatKI only impacts cortical bone and shifts the distribution towards the trabecular distribution with higher FAP values. One possible origin for this difference is the faster remodeling rate of trabecular bone relative to cortical bone. This difference in remodeling rate could alter the relative amounts of aligned/unaligned collagen and this could generate a difference in FAP value distribution. When considering only one type of bone at a time (cortical or trabecular), the drug treatment (ALN or CatKI) induces a different change in the FAP distribution relative to Sham. ALN and CatKI have different mechanisms of action that could potentially explain these differences. ALN binds to bone mineral and is taken into the osteoclast during bone resorption and induces apoptosis of the osteoclast (Drake et al., 2008). By way of contrast, CatKI inhibits cathepsin K, leading to reduction of osteoclastic bone resorption efficiency without a decrease in bone formation during bone remodeling (Pennypacker et al., 2011).

An important biological action of estrogen in bone is to induce apoptosis of osteoclasts (Weitzmann and Pacifici, 2006; Khosla et al., 2012). Estrogen depletion leads to the prolonged life of those cells and increased bone resorption. Increased bone formation simultaneously develops and an overall high-turnover state develops which leads to changes in bone quality and/or bone loss. Estrogen depletion led to changes in the distribution of FAP values for trabecular lumbar vertebrae but not cortical femur. Although the mechanism for this change is unknown, it could be related to the differences in estrogen receptors (ER). Trabecular bone primarily has the ERβ isoform and cortical bone primarily has the ERα isoform (Weitzmann and Pacifici, 2006). If estrogen signaling for apoptosis is selective for one isoform over the other, then this could potentially explain the FAP changes observed.

4.4. Relationship between FAP distributions and BMD

The bone mineral density (BMD) data for trabecular lumbar vertebrae samples in this rabbit study indicated a significant decrease in BMD for the OVX + Veh treatment as compared to Sham. The OVX + ALN and OVX + CatKI treatment groups showed no change in BMD (as compared to Sham control) (Pennypacker et al., 2011). The Sham and OVX + drug treatment samples all have the same BMD within error. The estrogen-depleted animals had a statistically significant lower BMD, as expected. The lumbar vertebrae samples imaged for the AFM analysis used lumbar vertebrae 4. Recall that the distributions of FAP values in trabecular bone showed a marginally significant shift towards lower values ($p = 0.07$), or more alignment, in response to OVX + Veh (Fig. 6). Under the OVX + CatKI treatment condition, both BMD and FAP values ($p = 0.89$) do not differ from Sham. Interestingly, under the OVX + ALN treatment condition (Fig. 6b), the BMD did not differ from Sham but the FAP values exhibited an increase (less alignment) that was marginally significant ($p = 0.054$). Additional work is needed to understand how these changes in BMD and FAP relate to bone quality and mechanical properties.

5. Conclusions

As expected, trabecular lumbar vertebrae had less aligned collagen than cortical femur in the Sham rabbits. The fibril alignment parameter (FAP) indicated that estrogen depletion in ovariectomized rabbits results in trabecular lumbar vertebrae and cortical femur having similar collagen fibril alignment. Drug treatments impact cortical femur and trabecular lumbar vertebrae differently. OVX + ALN treatment resulted in a change in FAP for both cortical femur and trabecular lumbar vertebrae. The cortical femur became more aligned and the trabecular lumbar vertebrae became less aligned. In contrast, OVX + CatKI did not result in changes in the distribution of alignment in trabecular lumbar vertebrae. The cortical femur, however, was shifted towards less alignment.

Estrogen depletion altered collagen fibril structure at different hierarchical levels for cortical and trabecular bone in rabbits. In rabbit cortical femur, OVX + Veh altered the formation of collagen bundles and sheets. In trabecular lumbar vertebrae, OVX + Veh altered collagen

fibril microstructure across a multimicron scale, as evidenced by the change in FAP value distribution. To effectively treat post-menopausal osteoporosis, it will be important for drug treatments to target the appropriate level of hierarchical structure being affected by the disease.

Disclosures

LTD is a current employee and may own stock/stock options of Merck & Co. MMBH received funding from the Merck Investigator Studies Program (MISP) for support of this research.

Authors' roles

Study Conception: MMBH, LTD. Study Design: MMBH, LTD, MAC, MM, JAF, KW, EDR. Study Conduct: MAC, MM, KW, MF. Data analysis and Interpretation: All authors. Drafting Manuscript: MAC, MM, MMBH. Revising and approving final version of manuscript: All authors. MMBH and MAC take responsibility for the integrity of the data.

Acknowledgments

Supported in part by a research grant to MMBH from the Investigator Initiated Studies Program of Merck Sharp & Dohme Corp (53294). The opinions expressed in this paper are those of the authors and do not necessarily represent those of Merck Sharp & Dohme Corp.

Appendix A. Supplementary data

Supplementary data to this article can be found online at http://dx.doi.org/10.1016/j.bonr.2016.08.003.

References

Black, D.M., Rosen, C., 2016. J. New Engl. J. Med. 374, 254.
Burr, D.B., 2002. Bone 31, 8.
Castaneda, S., Calvo, E., Largo, R., Gonzalez-Gonzalez, R., de la Piedra, C., Diaz-Curiel, M., Herrero-Beaumont, G., 2008. J. Bone Miner. Metab. 26, 53.
Cauble, M.A., Fang, M., Welch, K.B., Rothman, E.D., Pennypacker, B.L., Duong, L.T., Orr, B.G., Banaszak Holl, M.M., 2015. BoneKey 4, 697.
Diggle, P.J., Heagerty, P., Liang, K.-Y., Zeger, S.L., 2002. Analysis of Longitudinal Data. Oxford University Press.
Drake, M.T., Clarke, B.L., Khosla, S., 2008. Mayo Clin. Proc. 83, 1032.
Erickson, B., Fang, M., Wallace, J.M., Orr, B.G., Les, C.M., Banaszak Holl, M.M., 2013. Biotechnol. J. 8, 117.
Fang, M., Banaszak Holl, M.M., 2013. BoneKey 2, 394.
Fang, M., Liroff, K.G., Turner, A.S., Les, C.M., Orr, B.G., Banaszak Holl, M.M., 2012a. J. Invest. Dermatol. 132, 1791.
Fang, M., Goldstein, E.L., Turner, A.S., Les, C.M., Orr, B.G., Fisher, G.J., Welch, K.B., Rothman, E.D., Banaszak Holl, M.M., 2012b. ACS Nano 6, 9503.
Fang, M., Goldstein, E.L., Matich, E.K., Orr, B.G., Banaszak Holl, M.M., 2013. Langmuir 29, 2330.
Fantner, G.E., Rabinovych, O., Schitter, G., Thurner, P., Kindt, J.H., Finch, M.M., Weaver, J.C., Golde, L.S., Morse, D.E., Lipman, E.A., Rangelow, I.W., Hansma, P.K., 2006. Compos. Sci. Technol. 66, 1205.
Frost, H.M., Jee, W.S.S., 1992. Bone Miner. 18, 227.
Hassenkam, T., Fantner, G.E., Cutroni, J.A., Weaver, J.C., Morse, D.E., Hansma, P.K., 2004. Bone 35, 4.
Hassenkam, T., Jorgensen, H.L., Pedersen, M.B., Kourakis, A.H., Simonsen, L., Lauritzen, J.B., 2005. Micron 36, 681.
Johnell, O., Kanis, J.A., 2006. Osteoporos. Int. 17, 1726.
Kalu, D.N., 1991. Bone Miner. 15, 175.
Khosla, S., Oursler, M.J., Monroe, D.G., 2012. Trends Endocrinol. Metab. 23, 576.
Komori, T., 2015. Eur. J. Pharmacol. 759, 287.
Pennypacker, B.L., Duong, L.T., Cusick, T.E., Masarachia, P.J., Gentile, M.A., Gauthier, J.Y., Black, W.C., Scott, B.B., Samadfam, R., Smith, S.Y., Kimmel, D.B., 2011. J. Bone Miner. Res. 26, 252.
Smith, S.Y., Jolette, J., Turner, C.H., 2009. Am. J. Primatol. 71, 752.
Su, H.N., Ran, L.Y., Chen, Z.H., Qin, Q.L., Shi, M., Song, X.Y., Chen, X.L., Zhang, Y.Z., Xie, B.B., 2014. Nanoscale 6, 8134.
Troen, B.R., 2004. Drug News Perspect. 17, 19.
Viguet-Carrin, S., Garnero, P., Delmas, P.D., 2006. Osteoporos. Int. 17, 319.
Wallace, J.M., 2012. Bone 50, 420.
Wallace, J.M., Erickson, B., Les, C.M., Orr, B.G., Banaszak Holl, M.M., 2010a. Bone 46, 1349.
Wallace, J.M., Chen, Q., Fang, M., Erickson, B., Orr, B.G., Banaszak Holl, M.M., 2010b. Langmuir 26, 7349.
Weitzmann, M.N., Pacifici, R., 2006. J. Clin. Invest. 116, 1186.
Wright, N.C., Looker, A.C., Saag, K.G., Curtis, J.R., Delzell, E.S., Randall, S., Dawson-Hughes, B., 2014. J. Bone Miner. Res. 29, 2520.

Supplementary Material for

Estrogen depletion and drug treatment alters the microstructure of type I collagen in bone

Meagan A Cauble,[1] Matthew Muckley,[2] Ming Fang,[1] Jeffrey A Fessler,[2,3] Kathleen Welch,[4] Edward D Rothman,[4,5] Bradford G Orr,[6] Le T. Duong,[7] and Mark M Banaszak Holl[1,2,8]

[1]Department of Chemistry, University of Michigan, Ann Arbor, MI, USA [2]Department of Biomedical Engineering, University of Michigan, Ann Arbor, MI, USA [3]Electrical Engineering and Computer Science, University of Michigan, Ann Arbor, MI, USA. [4]Center for Statistical Consultation and Research (CSCAR), University of Michigan, Ann Arbor, MI. [5]Department of Statistics, University of Michigan, Ann Arbor, MI, USA. [6]Department of Physics, University of Michigan, Ann Arbor, MI, USA. [7]Bone Biology Group, Merck Research Laboratories, West Point, PA, USA. [8]Macromolecular Science and Engineering, University of Michigan, Ann Arbor, MI, USA.

Figure S1. Image of collagen, with arrows showing local alignment of collagen patches. The alignment was determined using an autocorrelation-based method. The arrow lengths are scaled to show the degree of alignment.

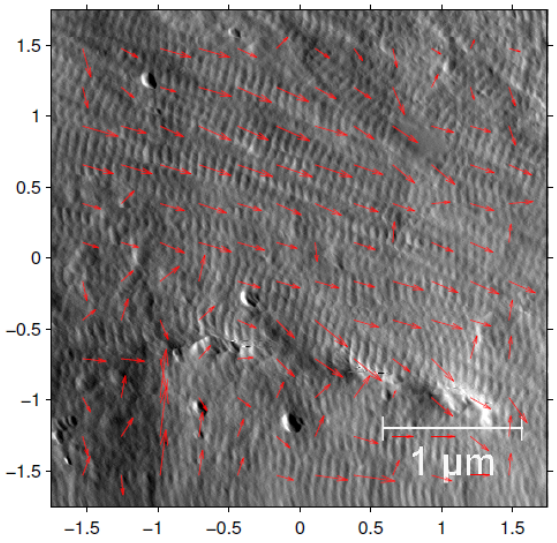

Figure S2. Image of collagen, with arrows showing local alignment of collagen patches. The alignment was determined using an autocorrelation-based method. The arrow lengths are scaled to show the degree of alignment.

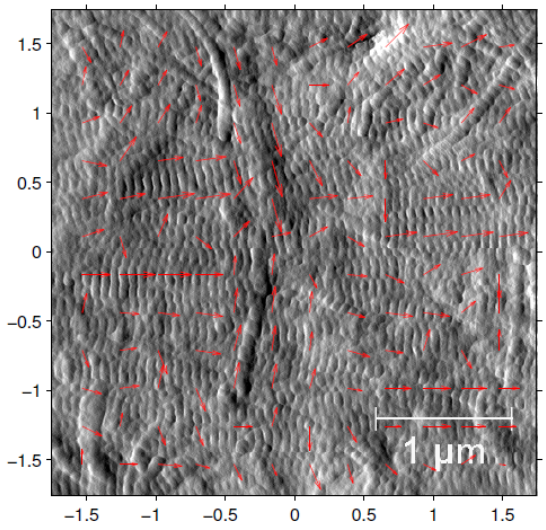

Figure S3 (a) A section of rabbit femur was taken from the diaphysis and mounted onto a steel puck. The remaining femur is shown behind the mounted sample. The mounted sample has been demarrowed, polished, and demineralized. (b) The rabbit lumbar vertebrae sections were taken from the caudal end of the vertebrae. The mounted sample pictured has been demarrowed, polished, and demineralized.

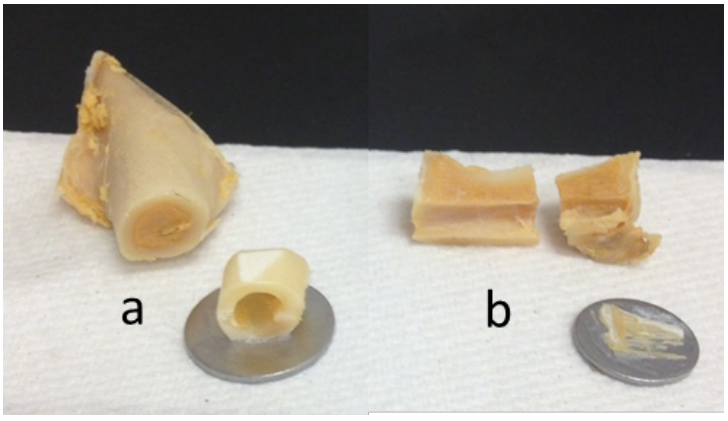

Figure S4. Summary of D-spacing data. a) Histogram of all D-spacings measured for lumbar trabeculae b) Boxplots of all D-spacings measured for lumbar trabeculae c) Cumulative distribution function (CDF) of all D-spacings measured for lumbar trabeculae. There is not a significant difference between the average D-spacing values or the distribution of all D-spacing values as assessed by the Kolmorgorov-Smirnov statistic of the CDF. See Cauble et al. 2015 for cortical femur data.

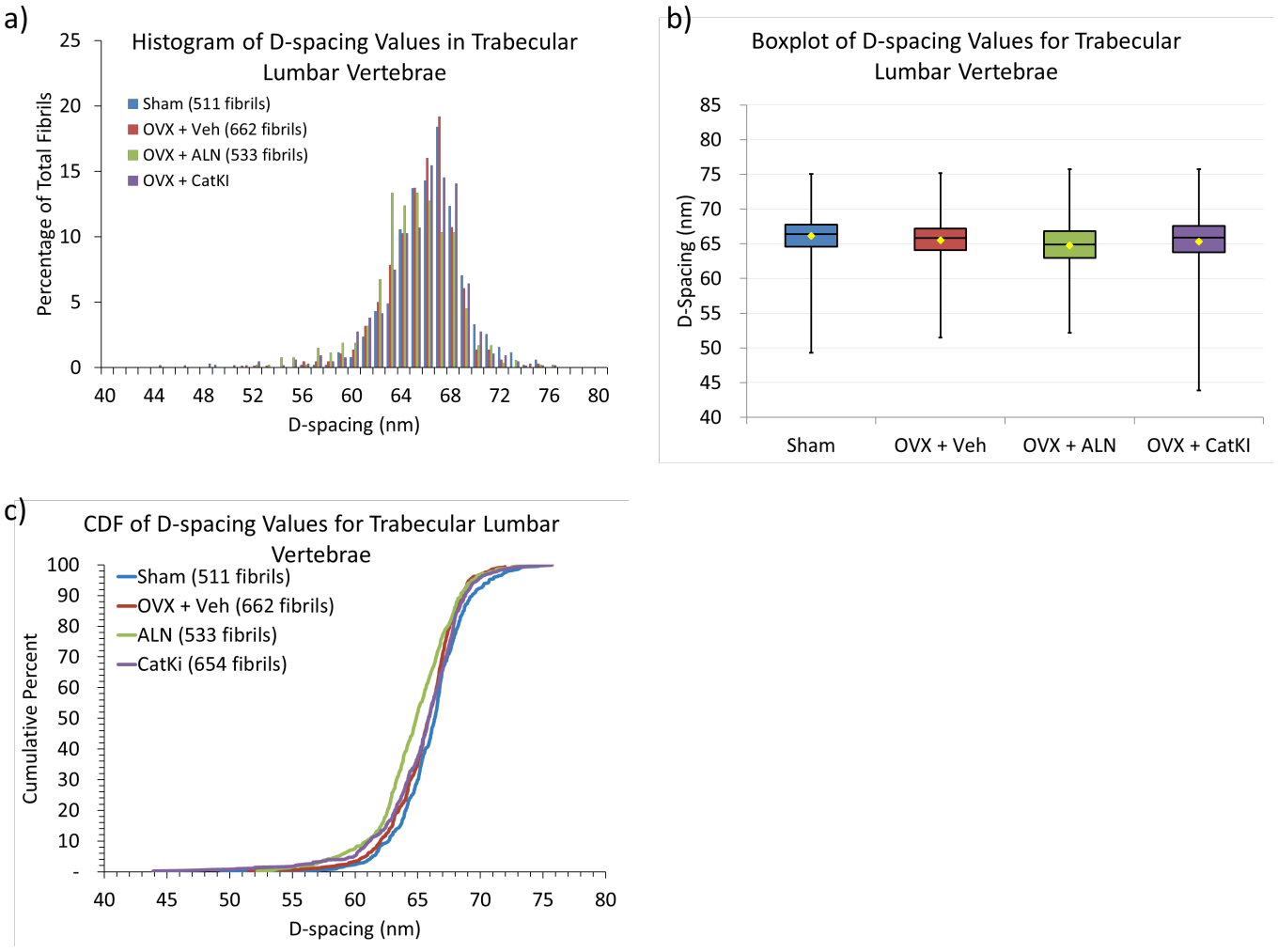

u

Figure S5: Cumulative distribution function plots of FAP values to show the difference between cortical femur and trabecular lumbar vertebrae (LV) for each of the four treatment groups. For all plots, the average FAP value is the same for cortical and trabecular samples. a) The distribution of FAP values for Sham cortical femur is shifted towards lower values (more aligned collagen) in comparison to Sham trabecular lumbar vertebrae. b) Estrogen depletion resulted in cortical femur and trabecular lumbar vertebrae producing the same average and the same distribution of FAP values. The similarity in the distribution of FAP values arises from estrogen depletion shifting trabecular lumbar vertebrae towards lower FAP values while not affecting the cortical femur FAP values (Figure 6). OVX + Veh is the only treatment group with this result. c) OVX + ALN shifted cortical femur towards lower FAP values and trabecular lumbar vertebrae towards higher FAP values (Figure 5 and 6). As a result, cortical femur has a distribution of FAP values that are lower than trabecular lumbar vertebrae but the distributions are farther apart than Sham. d) OVX + CatKI cortical femur also has a distribution of FAP values that is shifted towards lower values.

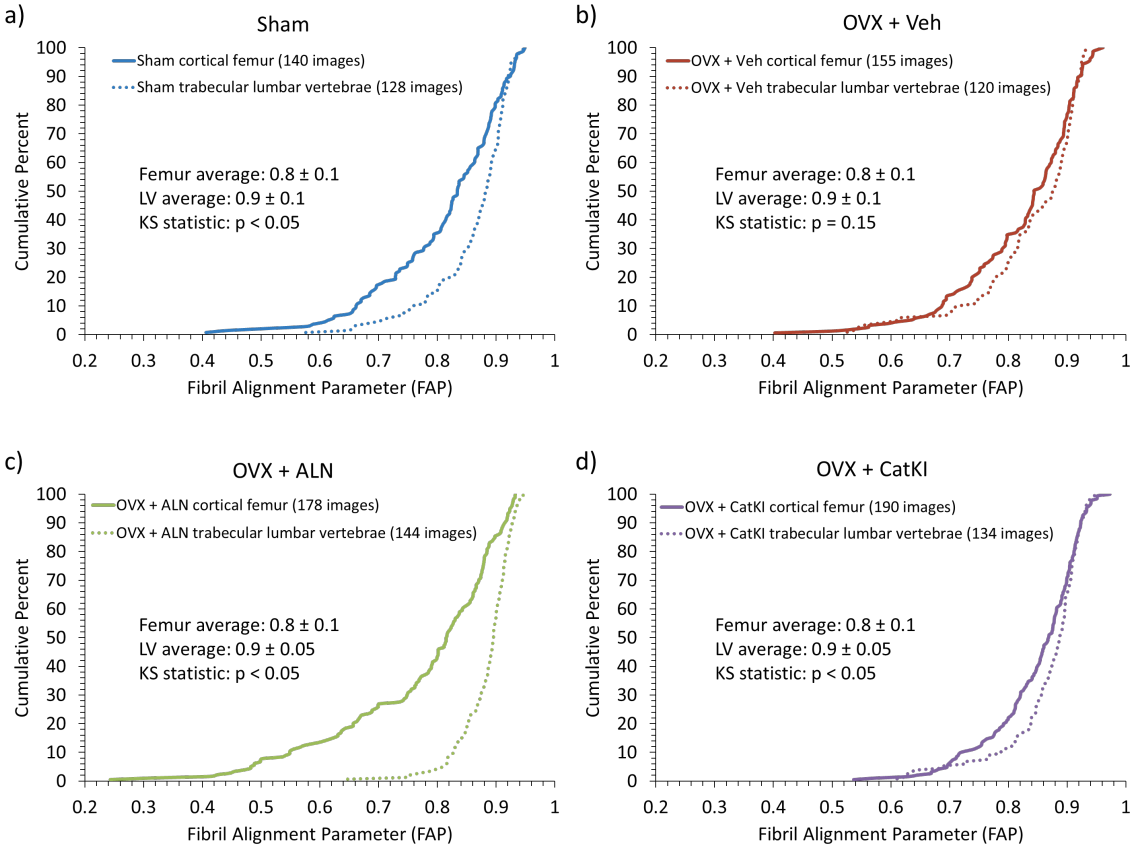

Table S1. Comparisons of the percentage of fibrils coded as *parallel* in cortical versus trabecular bone in each treatment group.

Comparison	p-value
Cortical Sham and Trabecular Sham	0.30
Cortical OVX + Veh and Trabecular OVX + Veh	0.06
Cortical OVX + ALN and Trabecular OVX + ALN	0.47
Cortical OVX + CatKI and Trabecular OVX + CatKI	0.13

Table S2. Comparisons of the percentage of fibrils coded as *oblique* in cortical versus trabecular bone in each treatment group.

Comparison	p-value
Cortical Sham and Trabecular Sham	0.20
Cortical OVX + Veh and Trabecular OVX + Veh	0.97
Cortical OVX + ALN and Trabecular OVX + ALN	0.79
Cortical OVX + CatKI and Trabecular OVX + CatKI	0.82